# CHAPTER 15
MTI RADAR

William W. Shrader
V. Gregers-Hansen
Equipment Division
*Raytheon Company*

15.1 INTRODUCTION TO MTI RADAR

The purpose of moving-target indication (MTI) radar is to reject signals from fixed or slow-moving unwanted targets, such as buildings, hills, trees, sea, and rain, and retain for detection or display signals from moving targets such as aircraft. Figure 15.1 shows a pair of photographs of a PPI (plan position indicator) which illustrate the effectiveness of a properly working MTI system. The distance from the center to the edge of the PPI is 40 nmi. The range marks are at 10-nmi intervals. The picture on the left is the normal video display, showing the fixed-target returns. The picture on the right shows the MTI clutter rejection. The camera shutter was left open for three scans of the antenna; thus aircraft show up as a succession of three returns.

MTI radar utilizes the doppler shift imparted on the reflected signal by a moving target to distinguish moving targets from fixed targets. In a pulse radar system this doppler shift appears as a change of phase of received signals between consecutive radar pulses. Consider a radar which transmits a pulse of RF energy that is reflected by both a building (fixed target) and an airplane (moving target) approaching the radar. The reflected pulses return to the radar a certain time later. The radar then transmits a second pulse. The reflection from the building occurs in exactly the same amount of time, but the reflection from the moving aircraft occurs in less time because the aircraft has moved closer to the radar in the interval between transmitted pulses. The precise time that it takes the reflected signal to reach the radar is not of fundamental importance. What is significant is whether the time changes between pulses. The time change, which is of the order of a few nanoseconds for an aircraft target, is determined by comparing the phase of the received signal with the phase of a reference oscillator in the radar. If the target moves between pulses, the phase of the received pulses changes.

Figure 15.2 is a simplified block diagram of one form of a coherent MTI system. The RF oscillator feeds the pulsed amplifier, which transmits the pulses. The RF oscillator is also used as a phase reference for determining the phase of reflected signals. The phase information is stored in a PRI (pulse repetition interval) memory for the period between transmitted pulses, and it is also subtracted
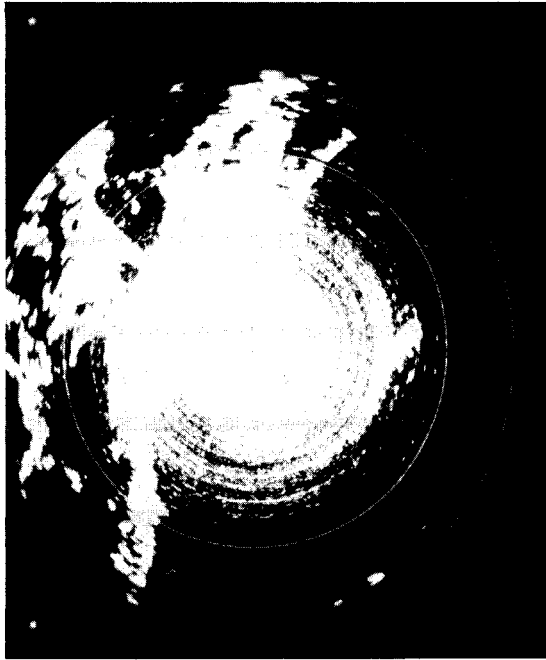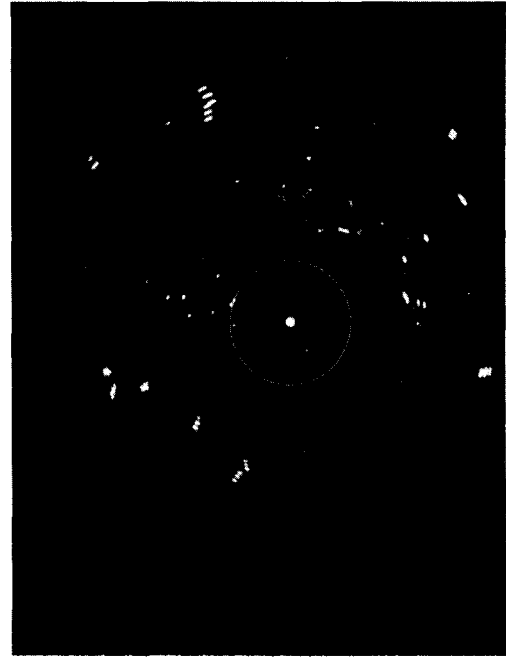
FIG. 15.1 (*a*) Normal video. (*b*) MTI video. These PPI photographs show how effective an MTI system can be. Aircraft appear as three consecutive blips in the right-hand picture because the camera shutter was open for three revolutions of the antenna. The PPI range is 40 nmi.
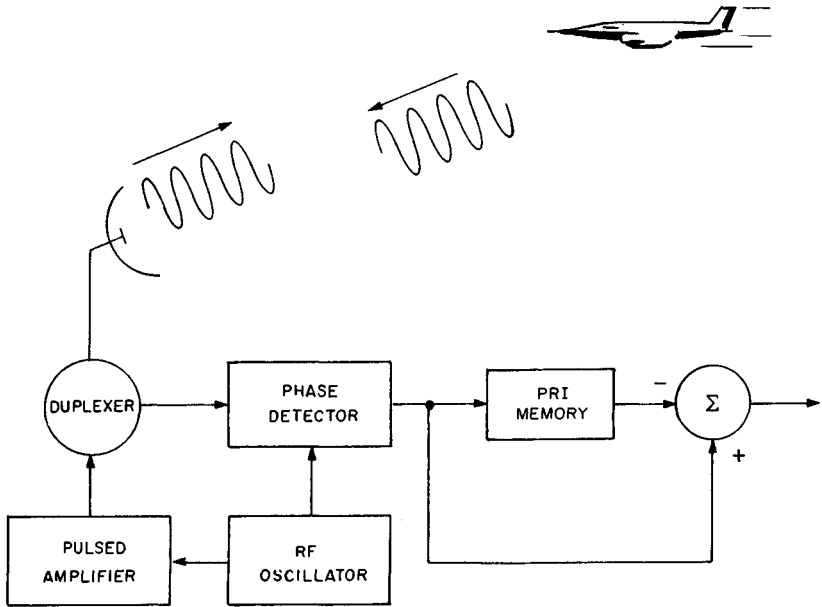
FIG. 15.2 Simplified block diagram of a coherent MTI system.

from the phase information from the previous transmitted pulse. There is an output from the subtractor only when a reflection has occurred from a moving target.

Moving-Target Indicator (MTI) Block Diagram. A block diagram of a complete MTI system is shown in Fig. 15.3. This block diagram represents an MTI system that uses a pulsed oscillator. It is not as sophisticated as MTI systems to be described later, but most of the practical considerations applying to any MTI system can be understood by examining this block diagram. The frequencies and 2500-μs interpulse period are typical for a 200-mi L-band radar.

The transmitter shown employs a magnetron. Because a magnetron is a pulsed oscillator that has no phase coherence between consecutive pulses, a phase reference must be established for each transmitted pulse. This is done by taking a sample of the transmitted pulse at a directional coupler, mixing this pulse with the stalo (stabilized local oscillator) and then using this pulse to phase-lock the coho (coherent oscillator). The coho then becomes the reference oscillator for the received signals. (The stability requirements for the coho and stalo will be described in Sec. 15.11.) The lock-pulse amplifier is gated off just before the end of the transmitted pulse because a magnetron emits a certain amount of noise during the fall of the high-voltage pulse applied to it, and this noise can prevent perfect locking of the coho.

The received signals are mixed with the stalo and amplified in a linear-limiting amplifier. (In some implementations the limiting is not deliberately provided. However, receiver saturation occurs at some signal level, and thus limiting inadvertently exists.)

The received signals are then compared in phase with the coho in a phase de-
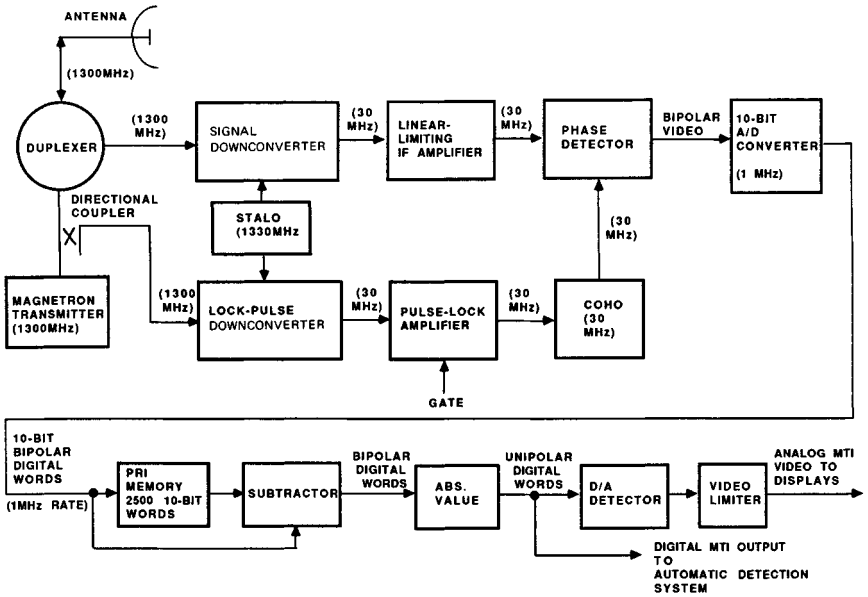
FIG. 15.3 MTI system block diagram.

tector. The output of the phase detector is a function of the relative phase of the signal and the coho, and it is also a function of the amplitude of the signal. At the output of the phase detector, the signal phase and amplitude information has been converted into bipolar video. The bipolar video received from a single transmitted pulse may appear as sketched in Fig. 15.4. If the point target is moving and if there is also a moving target in the region of strong clutter return, the superimposed bipolar video from several transmitted pulses may appear as in Fig. 15.5.

The remainder of the block diagram in Fig. 15.3 shows what is necessary for detecting the moving targets so that they may be displayed on a PPI or sent to an automatic target extractor. The bipolar video is converted to digital words in an analog-to-digital (A/D) converter. The A/D output is stored in a PRI memory and also subtracted from the memorized A/D output from the previous transmitted pulse.
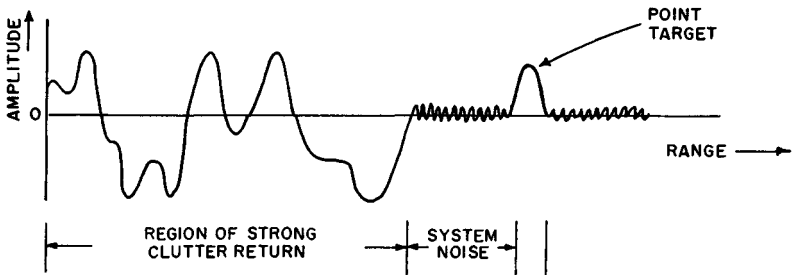

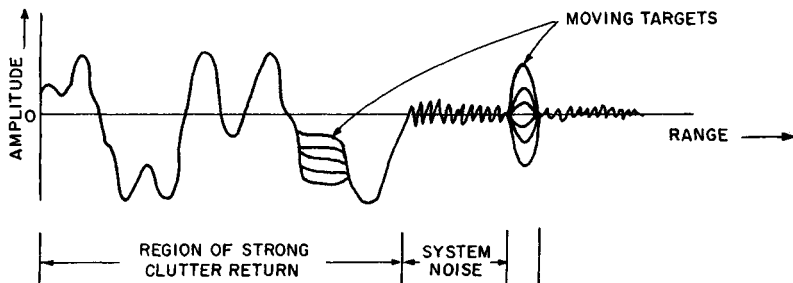**FIG. 15.4** Bipolar video: single sweep.

FIG. 15.5 Bipolar video: several sweeps.

The output of the subtractor is a digital bipolar signal that contains moving targets, system noise, and a small amount of clutter residue if clutter cancellation is not perfect. The absolute value of the signal is then converted to analog video in a digital-to-analog (D/A) converter for display on a PPI. The digital signal may also be sent to automatic target detection circuitry. The dynamic range (peak signal to rms noise) is limited to about 20 dB for a PPI display.

Moving-Target Detector (MTD) Block Diagram. In the moving-target detector (MTD) the basic MTI principle, as described above, is enhanced by increasing the linear dynamic range of the signal processor, using a number of parallel doppler filters followed by constant-false-alarm-rate (CFAR) processing, and adding one or more high-resolution clutter maps to suppress point clutter residues. With these additions a complete signal-processing system is obtained for suppressing clutter returns in a modern surveillance radar. A typical implementation of such an MTD processing system is shown in Fig. 15.6.

The MTD radar transmits a group of N pulses at a constant pulse repetition frequency (PRF) and at a fixed radar frequency. This set of pulses is usually referred to as the coherent processing interval (CPI) or pulse batch. Sometimes one or two additional fill pulses are added to the CPI in order to suppress range-ambiguous clutter returns, as might occur during periods of anomalous propagation. The returns received during one CPI are processed in the bank of N-pulse finite-impulse-response (FIR) filters. Then the radar may change PRF and/or RF
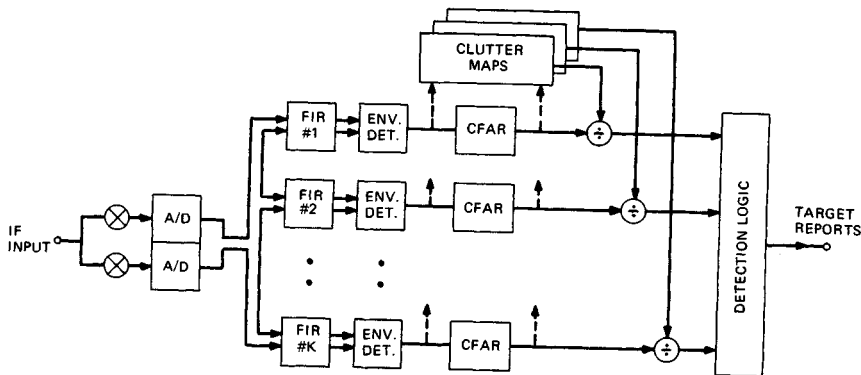

FIG. 15.6 MTD block diagram.

frequency and transmit another CPI of N pulses. Since most search radars are ambiguous in doppler, the use of different PRFs on successive coherent dwells will cause the target response to fall at different frequencies of the filter passband on the successive opportunities during the time on target, thus eliminating blind speeds.

Each doppler filter is designed to respond to targets in nonoverlapping portions of the doppler frequency band and to suppress sources of clutter at all other doppler frequencies. This approach maximizes the coherent signal integration in each doppler filter and provides clutter attenuation over a larger range of doppler frequencies than achievable with a single MTI filter. Thus one or more clutter filters may suppress multiple clutter sources located at different doppler frequencies. An example of the use of an MTD doppler filter bank against simultaneous land and weather clutter (Wx) is illustrated in Fig. 15.7. It can be seen that filters 3 and 4 will provide significant suppression of both clutter sources.
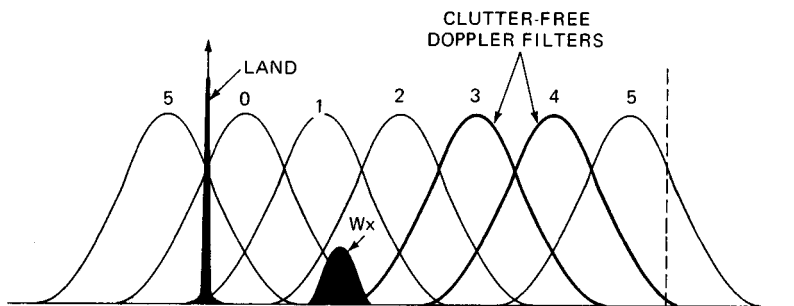

FIG. 15.7 Suppression of multiple clutter sources by using a doppler filter bank.

The output of each doppler filter is envelope-detected and processed through a cell-averaging CFAR processor to suppress residues due to range-extended clutter which may not have been fully suppressed by the filter.

As will be discussed later in this chapter, the conventional MTI detection system relies on a carefully controlled dynamic range in the IF section of the radar receiver in order to ensure that clutter residues at the MTI output are suppressed to the level of the receiver noise or below. This limited dynamic range, however, has the undesirable effect of causing additional clutter spectral broadening, and achievable clutter suppression is consequently reduced.

In the MTD one or more high-resolution clutter maps are used to suppress the clutter residues, after doppler filtering, to the receiver noise level (or, alternatively, to increase the detection threshold above the level of the residues). This in turn eliminates the need to restrict the IF dynamic range, which can then be set to the maximum value supported by the A/D converters. Thus, a system concept is obtained that provides a clutter suppression capability that is limited only by the radar system stability, the dynamic range of the receiver-processor, and the spectrum width of the returns from clutter. The concept of a high-resolution digital clutter map to suppress clutter residues is related to earlier efforts to construct analog area MTI systems using, for example, storage tubes.

In subsequent sections specific aspects of the design of an MTD system will be discussed. Thus Sec. 15.8 will discuss the design and performance of doppler filter banks, and a detailed discussion of clutter maps will follow in Sec. 15.14.

15.2 CLUTTER FILTER RESPONSE TO MOVING TARGETS

The response of an MTI system to a moving target varies as a function of the target's radial velocity. For the MTI system described above, the response, normalized for unity noise power gain, is shown in Fig. 15.8. Note that there is zero response to stationary targets and also to targets at ± 89, ± 178, $\pm 267, \ldots$ knots. These speeds, known as blind speeds, are where the targets move 0, $\frac{1}{2}$, 1, $1\frac{1}{2}, \ldots$ wavelengths between consecutive transmitted pulses. This results in the received signal being shifted precisely 360° or multiples thereof between pulses, which results in no change in the phase-detector output. The blind speeds can be calculated:

$$V_B = k\frac{\lambda f_r}{2} \qquad k = \pm 0, 1, 2, \ldots \qquad (15.1)$$

where V_B is the blind speed, in meters per second; λ is the transmitted wavelength, in meters; and f_r is the PRF, in hertz. A convenient set of units for this equation is

$$V_B\,(\text{kn}) = k\,\frac{0.29 f_r}{f_{\text{GHz}}} \qquad k = \pm 0, 1, 2, \ldots \qquad (15.2)$$

where f_r is the PRF, in hertz; and f_{GHz} is the transmitted frequency, in gigahertz. Note from the velocity response curve that the response to targets at velocities midway between the blind speeds is greater than the response for a normal receiver.

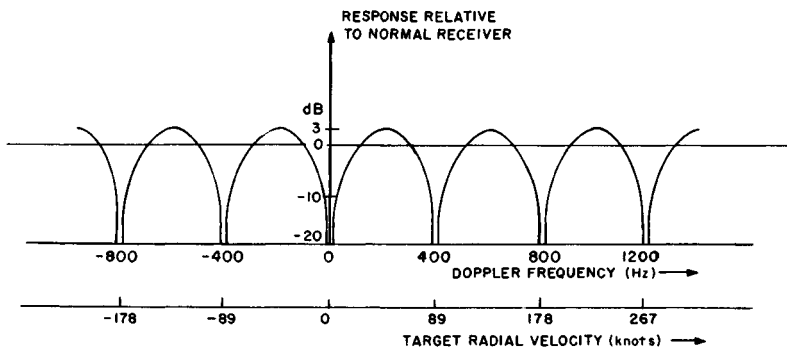The abscissa of the velocity response curve can also be labeled in terms of

FIG. 15.8 MTI system response for 1300-MHz radar operating at 400 pps.

doppler frequency. The doppler frequency of the target can be calculated from

$$f_d = \frac{2V_R}{\lambda}$$ (15.3)

where f_d is the doppler frequency, in hertz; V_R is the target radial velocity, in meters per second; and λ is the transmitted wavelength, in meters. It can be seen from Fig. 15.8 that the doppler frequencies for which the system is blind occur at multiples of the pulse repetition frequency.

15.3 CLUTTER CHARACTERISTICS

Spectral Characteristics. The spectrum of a pulsed transmitter transmitting a simple rectangular pulse of length τ is shown in Fig. 15.9. The spectral width of the (sin U)/U envelope is determined by the transmitted pulse width, the first nulls occurring at a frequency of $f_0 \pm 1/\tau$. The individual spectral lines are separated by a frequency equal to the PRF. These spectral lines fall at precisely the same frequencies as the blind speeds in Fig. 15.8. Thus a canceler will, in theory, fully reject signals with an ideal spectrum, as shown here. In practice, however, the spectral lines in clutter signals are broadened by motion of the clutter (such as windblown trees) and by motion of the antenna in a scanning radar. Barlow[1] stated that the returns from clutter have a gaussian spectrum, which may be characterized by its standard deviation σ_v. This spectral spread prevents perfect cancellation of clutter in the MTI system.
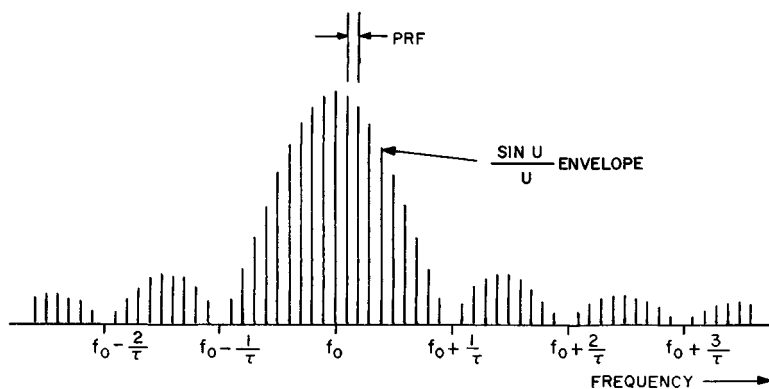

FIG. 15.9 Pulse transmitter spectrum.

Table 15.1 gives the standard deviation σ_v of the clutter spectrum in meters per second. More sophisticated and detailed clutter spectrum models exist,[6] but the gaussian model is usually an adequate model for understanding system limitations and obtaining good performance predictions.

Nathanson and Reilly[7] have shown that the clutter spectral width of rain is primarily due to a turbulence component and a wind-shear component (change in

TABLE 15.1   Summary of Standard Deviations of the Clutter Spectrum*

Source of clutter	Wind speed, kn	σ_v, m/s	Reference
Sparse woods	Calm	0.017	Barlow[1]
Wooded hills	10	0.04	Goldstein,[3] pp. 583–585
Wooded hills	20	0.22	Barlow[1]
Wooded hills	25	0.12	Goldstein,[3] pp. 583–585
Wooded hills	40	0.32	Goldstein,[3] p. 583
Sea echo		0.7	Wiltse et al.,[4] p. 226
Sea echo		0.75–1.0	Goldstein,[3] pp. 580–581
Sea echo	8–20	0.46–1.1	Hicks et al.,[5] p. 831
Sea echo	Windy	0.89	Barlow[1]
Chaff		0.37–0.91	Goldstein,[3] p. 472
Chaff	25	1.2	Goldstein,[3] p. 472
Chaff		1.1	Barlow[1]
Rain clouds		1.8–4.0	Goldstein,[3] p. 576
Rain clouds		2.0	Barlow[1]

*From Barton.[2]

wind velocity with altitude). Their measurements indicate that good average values are $\sigma_v = 1.0$ m/s for turbulence and $\sigma_v = 1.68$ m/(s/km) for wind shear. A convenient equation is $\sigma_v = 0.04R\theta_{el}$ m/s for the effects of wind shear, provided the rain fills the vertical beam, where R is the range to the weather, in nautical miles; and v_{el} is the one-way half-power vertical beamwidth, in degrees. Thus, for example, σ_v of rain viewed at 25 nmi with a vertical beamwidth of 4° would have a $\sigma_v = 4.1$ m/s, of which the shear component is dominant. Rain and chaff also have an average velocity, in addition to the spectral spread noted above, which must be taken into account when designing an MTI system.

The clutter spectral width in meters per second is independent of the radar frequency. The standard deviation of the clutter power spectrum σ_c, in hertz, is

$$\sigma_c = \frac{2\sigma_v}{\lambda} \quad \text{Hz} \tag{15.4}$$

where λ is the transmitted wavelength, in meters; and σ_v is the clutter standard deviation, in meters per second.

Antenna scanning also causes a spread of the clutter power spectrum because of amplitude modulation of the echo signals by the two-way antenna pattern.[2] The resulting clutter standard deviation is

$$\sigma_c = \frac{\sqrt{\ln 2}}{\pi} \times \frac{f_r}{n} = 0.265 \frac{f_r}{n} \quad \text{Hz} \tag{15.5}$$

where f_r is the PRF and n is the number of hits between the one-way 3 dB points of the antenna pattern. This equation was derived for a gaussian beam shape but is essentially independent of the actual beam shape or aperture illumination function used.

The clutter spectral spread due to scanning, normalized to the PRF, is

$$\sigma_c T = \frac{0.265}{n} \qquad (15.6)$$

where $T = 1/\text{PRF}$ is the interpulse period.

Amplitude Characteristics. To predict the performance of an MTI system, the amplitude of the clutter signals with which a target must compete should be known. The amplitude of the clutter signals is dependent on the size of the resolution cell of the radar, the frequency of the radar, and the reflectivity of the clutter. The expected radar cross section of clutter can be expressed as the product of a reflectivity factor and the size of the volume or area of the resolution cell.

For surface clutter, as viewed by a surface-based radar,

$$\bar{\sigma} = A_c \sigma^0 = R\theta_{\text{az}} \frac{c\tau}{2} \sigma^0 \qquad (15.7)$$

where $\bar{\sigma}$ is the average radar cross section, in square meters; A_c is the area of clutter illuminated, in square meters; R is the range to clutter patch, in meters; θ_{az} is the one-way half-power azimuthal beamwidth, in radians; c is the speed of propagation, 300 million m/s; τ is the half-power radar pulse length (after the matched filter), in seconds; and σ^0 is the average clutter reflectivity factor, in square meters per square meter.

For clutter that is airborne, such as chaff or rain,

$$\bar{\sigma} = V_c \eta = R\theta_{\text{az}} H \frac{c\tau}{2} \eta \qquad (15.8)$$

where V_c is the volume of clutter illuminated, in cubic meters; H is the height of clutter, in meters (if clutter fills the vertical beam, then $H = R\theta_{\text{el}}$, where θ_{el} is the elevation beamwidth); and η is the clutter reflectivity factor, in square meters per cubic meter.

It should be noted that, for land clutter, σ^0 can vary considerably from one resolution cell to the next. A typical distribution of σ^0, taken from Barton,[8] is shown in Fig. 15.10. Typical values for σ^0 and η taken from the same reference are given in Table 15.2. Because of the imprecision in predicting σ^0 and η, these equations do not include an antenna beam-shape factor. For the measurement of the reflectivity of rain, references on radar meteorology present more precise equations.[9]

In addition to distributed clutter targets, there are many targets that appear as *points*, such as radio towers, water tanks, and buildings. These point targets typically have a radar cross section of 10^3 to 10^4 m^2.

Figure 15.11*a* shows a PPI display of all clutter observed with a surveillance radar with a 1.3° by 2-μs resolution cell in the mountainous region of Lakehead, Ontario, Canada. (The PPI range is set for 30 nmi.) Clutter that exceeds the minimum-discernible signal (MDS) level of the radar by 60 dB is shown in Fig. 15.11*b*. Note that the clutter in Fig. 15.11*b* is very spotty in character, including the strong fixed-point targets and returns from extended targets. It is significant that the extended targets are no longer very extended. The face of a mountain at 10 mi from 5 to 7 o'clock is only a line. If the MTI system were incapable of displaying an aircraft while it was over the mountain face, it would display the aircraft on the next scan of the antenna because the aircraft would have moved either farther or nearer. The PPI does not have a resolution that approaches the resolution of the signal-processing
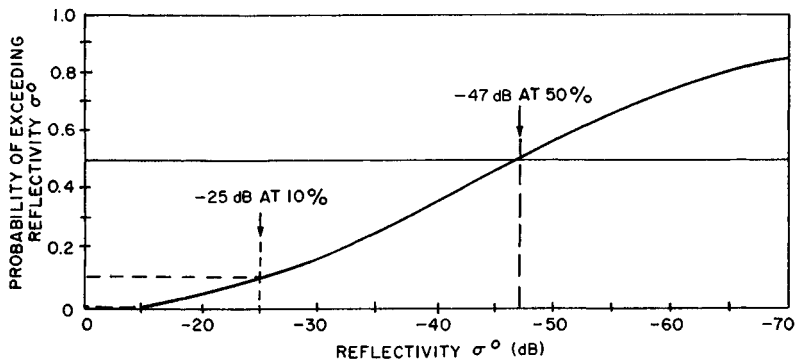
FIG. 15.10 Distribution of reflectivity for ground clutter typical of heavy clutter at S band.

circuits of this radar. Thus the apparent extended clutter has many weak areas not visible in these photographs, where targets could be detected by virtue of an MTI radar's interclutter visibility (defined in Sec. 15.4).

15.4 DEFINITIONS

Improvement Factor (I).   The MTI improvement factor I is defined as "the signal-to-clutter ratio at the output of the clutter filter divided by the signal-to-clutter ratio at the input of the clutter filter, averaged uniformly over all target radial velocities of interest."[10] This definition accounts for both the clutter attenuation and the average noise gain of the MTI system. It is therefore a measure of the MTI system response to clutter relative to the average MTI system response to targets. An equivalent definition of improvement factor is $I = r_i/r_o$, where r_i is the input ratio of clutter to noise and r_o is the output ratio of clutter residue to noise. The use of I is encouraged instead of older terms, such as *cancellation ratio* and *clutter attenuation*, because these terms have not been consistently used in the literature and are not always normalized to the average canceler noise gain.

Signal-to-Clutter Ratio Improvement (I_{SCR}).   For a system employing multiple doppler filters, such as the MTD, each filter will have a different improvement factor against the same clutter source. In this case it is preferable to define the performance against clutter in terms of the signal-to-clutter improvement (I_{SCR}) versus target doppler shift. This quantity is not included in the *IEEE Dictionary*,[10] but common usage defines the I_{SCR}, at each target doppler frequency, as the ratio of the signal-to-clutter ratio obtained at the output of the doppler filter bank (including all filters) to the signal-to-clutter ratio at the input of the filter bank. It should be noted that the signal-to-clutter improvement of any one filter is equal to the product of the MTI improvement factor of the filter as defined earlier and the coherent gain of the filter at the particular doppler frequency. The coherent gain of a doppler filter is equal to the increase in signal-to-thermal-noise ratio between the input and the output of the filter due to the coherent summation of individual target returns.

TABLE 15.2 Typical Values of Clutter Reflectivity*

| Clutter	Reflectivity, λ, m η, $(\text{m})^{-1}$	Conditions	Band λ, m	Clutter parameters for typical conditions			
				L 0.23	S 0.1	C 0.056	X 0.032
Land (excluding point clutter)	$\sigma^0 = \dfrac{0.00032}{\lambda}$ (worst 10 percent)	. . . .	σ^0 dB =	-29	-25	-22	-20
Point clutter	$\sigma = 10^4$ m^2	. . . .	σ m^2 =	10^4	10^4	10^4	10^4
Sea (Beaufort scale K_B, angle E)	σ^0 dB = $-64 + 6K_B$ + $(\sin E)$dB $- \lambda$ dB	Sea state 4 (6-ft waves, rough); $E = 1°$	σ^0 dB =	-51.5	-47.5	-44.5	-42.5
Chaff (for fixed weight per unit volume)	$\eta = 3 \times 10^{-8}\lambda$	. . . .	η (m)$^{-1}$ =	7×10^{-9}	3×10^{-9}	1.7×10^{-9}	10^{-9}
Rain (for rate r, mm/h)	$\eta = 6 \times 10^{-14}r^{1.6}\lambda^{-4}$ (matched polarization)	$r = 4$ mm/h	η (m)$^{-1}$ =	2×10^{-10}	5×10^{-9}	5×10^{-8}	5×10^{-7}

*From Barton.[8]
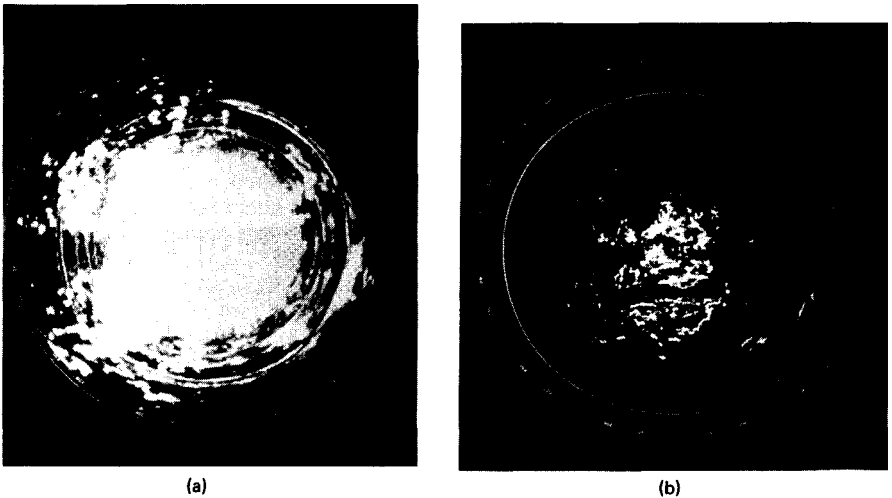
FIG. 15.11 PPI display, 30-nmi range, of (*a*) all clutter at a mountainous site and (*b*) clutter that exceeds the system noise level by 60 dB.

Subclutter Visibility (SCV). The subclutter visibility (SCV) of a radar system is a measure of its ability to detect moving-target signals superimposed on clutter signals. A radar with 20 dB SCV can detect an aircraft flying over clutter whose signal return is 100 times stronger. The *IEEE Dictionary*[10] defines the subclutter visibility as "the ratio by which the target echo power may be weaker than the coincident clutter echo power and still be detected with specified detection and false alarm probabilities. Target and clutter powers are measured on a single pulse return and all target radial velocities are assumed equally likely." The SCV of two radars cannot necessarily be used to compare their performance while operating in the same environment, because the target-to-clutter ratio seen by each radar is proportional to the size of the radar resolution cell and may also be a function of frequency. Thus a radar with a 10-μs pulse length and a 10° beamwidth would need 20 dB more subclutter visibility than a radar with a 1-μs pulse and a 1° beamwidth for equal performance in a specified clutter environment.

The subclutter visibility of a radar, when expressed in decibels, is less than the improvement factor by the clutter visibility factor V_{oc} (see definition below).

Interclutter Visibility (ICV). The interclutter visibility (ICV) of a radar is a measure of its capability to detect targets between points of strong clutter by virtue of the ability of the radar to resolve the areas of strong and weak clutter. A radar with high resolution makes available regions between points of strong clutter where the target-to-clutter ratio will be sufficient for target detection even though the SCV of the radar (based on average clutter) may be relatively low. A low-resolution radar averages the clutter over large resolution cells, most of which will contain one or more strong point targets, and thus the radar will have very little ICV. Because of the ICV capability of high-resolution radars, they tend to perform better in a clutter environment than would be predicted by using the average clutter amplitude characteristics of Sec. 15.3.[11] To achieve ICV, a mechanism must be furnished to provide CFAR operation

against the residue from strong clutter. This CFAR is provided in the typical MTI system by IF limiting or, in the MTD implementation, through the use of high-resolution clutter maps.

Filter Mismatch Loss. The maximum signal-to-noise ratio available from an N-pulse filter is N times the signal-to-noise ratio of a single pulse, assuming all pulses have equal amplitude. When weighting is applied to reject clutter and control the filter sidelobes, the peak output signal-to-noise ratio is reduced. The filter mismatch loss is the amount by which the peak-output signal-to-noise ratio is reduced by the use of the weighting. A three-pulse MTI filter using binomial weights has a filter mismatch loss of 0.51 dB. The mismatch loss for the binomial-weighted four-pulse canceler is 0.97 dB.

Clutter Visibility Factor (V_{oc}). This factor is "the predetection signal-to-clutter ratio that provides stated probabilities of detection and false alarm on a display; in moving-target-indicator systems, it is the ratio after cancelation or doppler filtering."[10] The clutter visibility factor is the ratio by which the target signal must exceed the clutter residue so that target detection can occur without having the clutter residue result in false-target detections. The system must provide a threshold that the targets will cross and the clutter residue will not cross.

15.5 IMPROVEMENT FACTOR CALCULATIONS

Using Barton's approach (Ref. 2, pp. 210–219), the maximum improvement factor I against zero-mean clutter with a gaussian-shaped spectrum, for different implementations of the finite-impulse-response binomial-weight MTI canceler (see Sec. 15.7), is

$$I_1 \approx 2\left(\frac{f_r}{2\pi\sigma_c}\right)^2 \tag{15.9}$$

$$I_2 \approx 2\left(\frac{f_r}{2\pi\sigma_c}\right)^4 \tag{15.10}$$

$$I_3 \approx \frac{4}{3}\left(\frac{f_r}{2\pi\sigma_c}\right)^6 \tag{15.11}$$

where I_1 is the MTI improvement factor for the single-delay coherent canceler; I_2 is the MTI improvement factor for the dual-delay coherent canceler; I_3 is the MTI improvement factor for the triple-delay coherent canceler; σ_c is the rms frequency spread of the gaussian clutter power spectrum, in hertz; and f_r is the radar repetition frequency, in hertz. When the values of σ_c for scanning modulation [Eq. (15.5)] are substituted in the above equations for I, the limitation on I due to scanning is

$$I_1 \approx \frac{n^2}{1.39} \tag{15.12}$$

$$I_2 \approx \frac{n^4}{3.84} \tag{15.13}$$

$$I_3 \approx \frac{n^6}{16.0} \tag{15.14}$$

These relationships are shown graphically in Fig. 15.12. This derivation assumes a linear system. That is, it is assumed that the voltage envelope of the echo signals, as the antenna scans past a point target, is identical to the two-way antenna voltage pattern. This assumption of a linear system may be unrealistic for some practical MTI systems with relatively few hits per beamwidth, as discussed in Sec. 15.10.

The scanning limitation does not apply to a system that can step-scan, such as a phased array. Note, however, that sufficient pulses must be transmitted to initialize the filter before useful outputs may be obtained. For example, with a three-pulse binomial-weight canceler, the first two transmitted pulses initialize the canceler, and useful output is not available until after the third pulse has been transmitted. Feedback or infinite impulse response (IIR) filters would not be used with a step-scan system because of the long transient settling time of the filters.

The limitation on I due to internal-clutter fluctuations can be determined by substituting the appropriate value of σ_c into Eqs. (15.9) to (15.11). By letting $\sigma_c = 2\sigma_v/\lambda$, where σ_v is the rms velocity spread of the clutter, the limitation on I can be plotted for different types of clutter as a function of the wavelength λ and the pulse repetition frequency f_r. This is done for one-, two-, and three-delay binomial-weight cancelers in Figs. 15.13 to 15.15. The values of V_B given are the first blind speed of the radar (or where the first blind speed V_B would be for a staggered PRF system if staggering were not used). The improvement factor
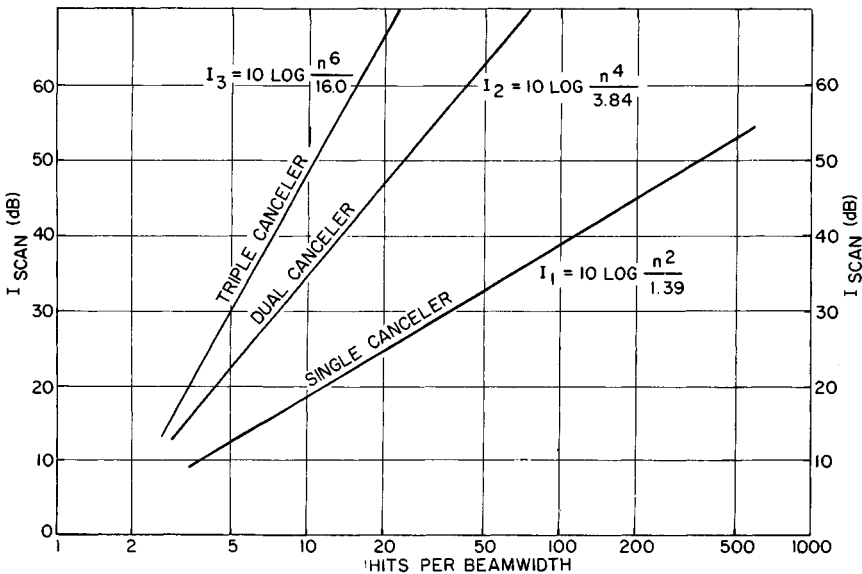

FIG. 15.12 Theoretical MTI improvement factor due to scan modulation; gaussian antenna pattern; n = number of pulses within the one-way half-power beamwidth.
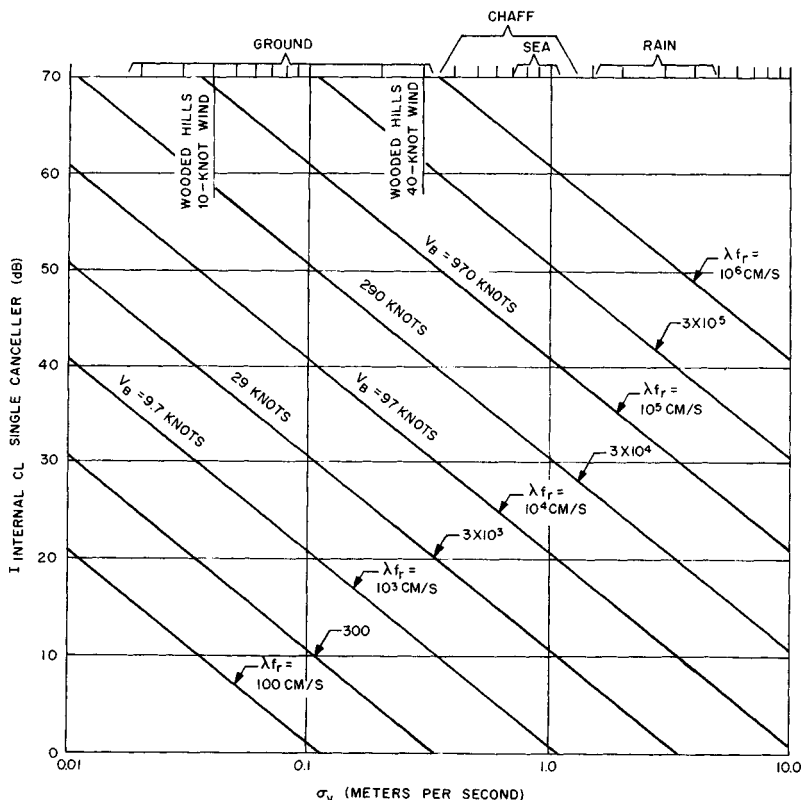
FIG. 15.13 MTI improvement factor as a function of the rms velocity spread of clutter for a two-pulse binomial-weight canceler.

shown in these figures for rain and chaff is based on the assumption that the average velocity of the rain and chaff has been compensated for so that the returns are centered in the canceler rejection notch. Unless such compensation is provided, the MTI offer little or no improvement for rain and chaff.

Two further limitations on I are the effect of pulse-to-pulse repetition-period staggering combined with clutter spectral spread from scanning and internal-clutter motion. These limitations, plotted in Figs. 15.16 and 15.17, apply to all cancelers, whether single or multiple. (The derivation of these limitations and a means of avoiding them by the use of time-varying weights are given in Sec. 15.9.)

15.6 OPTIMUM DESIGN OF CLUTTER FILTERS

The statistical theory of detection of signals in gaussian noise provides the required basis for the optimum design of radar clutter filters. Such theoretical results are important to the designer of a practical MTI or MTD system, in that
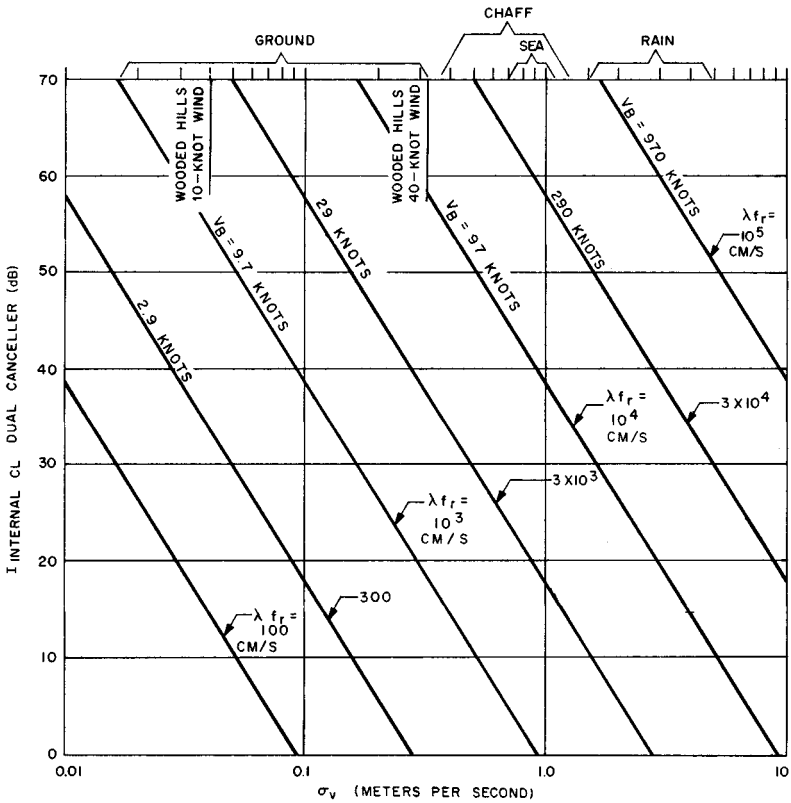
FIG. 15.14 MTI improvement factor as a function of the rms velocity spread of clutter for a three-pulse binomial-weight canceler.

they establish upper bounds on the achievable performance in a precisely specified clutter environment. It should be noted, however, that owing to the extreme variability of the characteristics of real clutter returns (power level, doppler shift, spectrum shape, spectral width, etc.) any attempt to actually approximate the performance of such optimum filters for the detection of targets in clutter requires the use of adaptive methods. The adaptive methods must estimate the unknown clutter statistics and subsequently implement the corresponding optimum filter. The design of such adaptive MTI systems is discussed in Sec. 15.13.

For a single radar pulse with a duration of a few microseconds, the doppler shift due to aircraft target motion is a small fraction of the signal bandwidth, and conventional MTI and pulse doppler processing are not applicable. It is well known that the classical single-pulse "matched" filter provides optimum radar detection performance when used in a white-noise background. Against clutter returns which have the same spectrum as the transmitted radar pulse, the matched filter is no longer optimum, but the potential improvement in the output signal-to-clutter ratio by designing a modified optimized filter is usually insignificant.

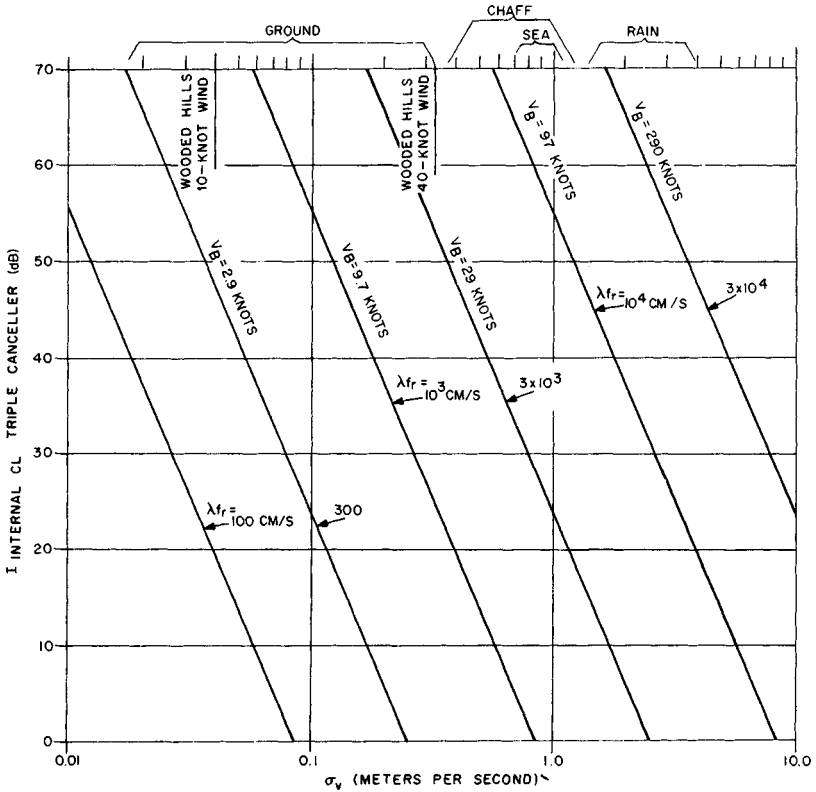When the duration of the transmitted radar signal, whether CW or a repetitive

FIG. 15.15 MTI improvement factor as a function of the rms velocity spread of clutter for a four-pulse binomial-weight canceler.

train of N identical pulses, is comparable with or larger than the reciprocal of anticipated target doppler shifts, the difference between a conventional white-noise matched filter (or coherent integrator) and a filter optimized to reject the accompanying clutter becomes significant. The characteristics of the clutter are characterized by the covariance matrix Φ_C of the N clutter returns. If the power spectrum of the clutter is denoted $S_C(f)$ and the corresponding autocorrelation function is $R_C(t_i - t_j)$, then the elements of Φ_C are given by

$$\Phi_{ij} = R_C(t_i - t_j) \tag{15.15}$$

where t_i is the transmission time of the ith pulse. For example, for a gaussian-shaped clutter spectrum we have

$$S_C(f) = P_C \frac{1}{\sqrt{2\pi}\,\sigma_f} \exp\left[-\frac{(f - f_d)^2}{2\sigma_f^2}\right] \tag{15.16}$$

where P_C is the total clutter power, σ_f is the standard deviation of the clutter
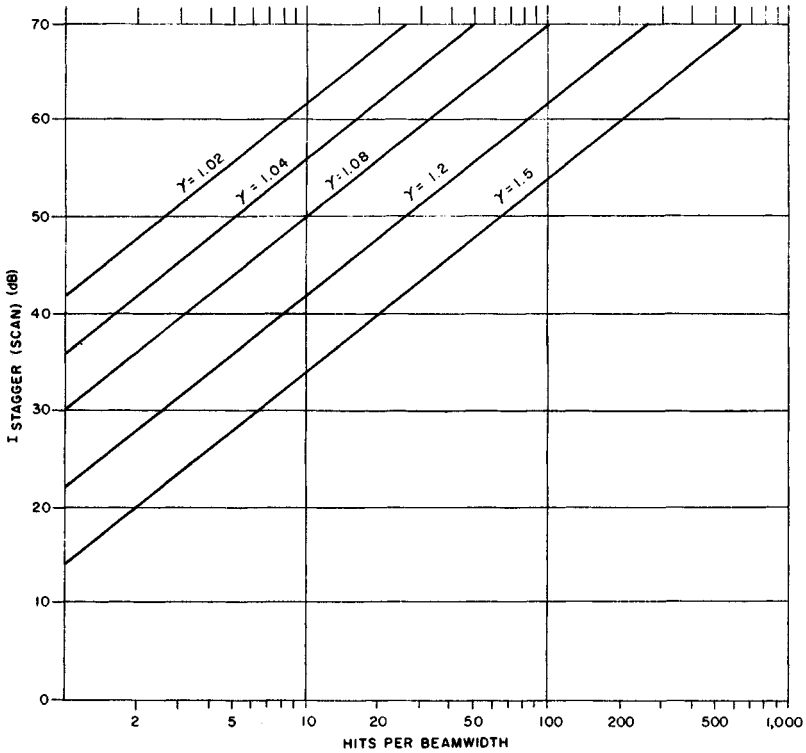
FIG. 15.16 Approximate MTI improvement factor limitation due to pulse-to-pulse repetition-period staggering and scanning (all canceler figurations). $I(\text{dB}) = 20 \log [2.5n/(\gamma - 1)]$; γ = maximum period/minimum period.

spectral width, and f_d is the average doppler shift of the clutter. The corresponding autocorrelation function is

$$R_C(\tau) = P_C \exp(-4\pi\sigma_f^2\tau^2) \exp(-j2\pi f_d\tau) \qquad (15.17)$$

For two pulses separated in time by the interpulse period T the complex correlation coefficient between two clutter returns is

$$\rho_T = \exp(-4\pi\sigma_f^2 T^2) \exp(-j2\pi f_d T) \qquad (15.18)$$

The second factor in this expression represents the phase shift caused by the doppler shift of the clutter returns.

For a known target doppler shift the received target return can be represented by an N-dimensional vector:

$$s = P_S\mathbf{f} \qquad (15.19)$$

where the elements of the vector $\mathbf{f}$ are $f_i = \exp[j2\pi f_s t_i]$. On the basis of this de-
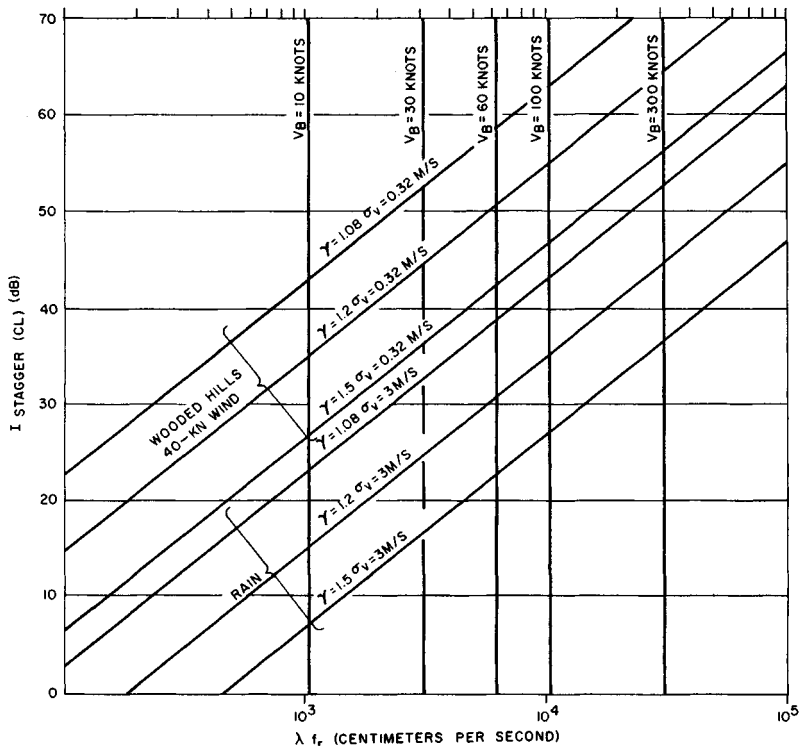
FIG. 15.17 Approximate MTI improvement factor limitation due to pulse-to-pulse staggering and internal-clutter motion (all canceler configurations). $I(\text{dB}) = 20 \log [0.33/(\gamma - 1)(\lambda f_r/\sigma_v)]$; γ = maximum period/minimum period.

scription of signal and clutter it has been shown[12] that the optimum doppler filter will have weights given by

$$w_{\text{opt}} = \Phi_C^{-1} s \tag{15.20}$$

and the corresponding signal-to-clutter improvement is

$$I_{\text{SCR}} = \frac{w_{\text{opt}}{}^T s \cdot s^{T^*} w_{\text{opt}}{}^*}{w_{\text{opt}}{}^T \Phi_C w_{\text{opt}}{}^*} \tag{15.21}$$

where the asterisk denotes complex conjugation and superscript T is the transposition operator. An example where the optimum performance is determined for the case of clutter at zero doppler having a wide gaussian-shaped spectrum and a normalized width of $\sigma_f T = 0.1$ is shown in Fig. 15.18. In this case a coherent processing interval of CPI = nine pulses was assumed, and the limitation due to thermal noise was ignored by setting the clutter level at 100 dB above noise.

It should be kept in mind that Eq. (15.21) for the optimum weights will yield a different result for each different target doppler shift, so that a large number of
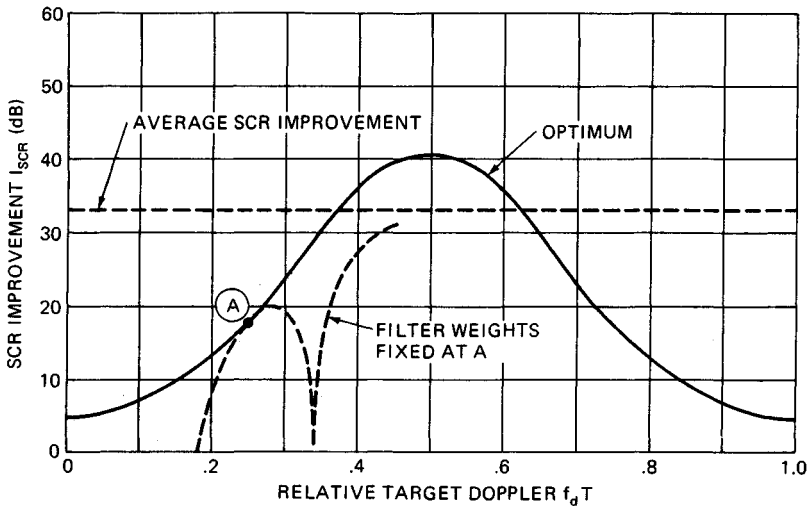
FIG. 15.18 Optimum signal-to-clutter ratio improvement (I_{SCR}) for gaussian-shaped clutter spectrum and a CPI of nine pulses; clutter-to-noise ratio, 100 dB.

parallel filters would be needed to approximate the optimum performance even when the clutter characteristics are known exactly. As an example, the response of the optimum filter designed for one particular target doppler frequency labeled as point A in Fig. 15.18 is shown in a broken line. At approximately ±5 percent from the design doppler the performance starts to fall significantly below the optimum.

Also shown in Fig. 15.18 is a horizontal line labeled "average SCR improvement." This indicates the level corresponding to the average of the optimum SCR curve across one doppler interval and may be considered as a figure of merit for a multiple-filter doppler processor somewhat analogous to the MTI improvement factor defined for a single doppler filter. In Fig. 15.19 the optimum average I_{SCR} has been computed for several different values of the CPI as a function of the normalized spectrum width. These results may be used as a point of reference for practical doppler processor designs as discussed in Sec. 15.8. Note that for $\sigma_f T \approx 1$ the average SCR improvement is due only to the coherent integration of all the pulses in the CPI.

The implementation of a single MTI filter will result in a performance below that shown in Fig. 15.19. Further, it can be shown that the average SCR improvement calculated for a single filter is equal to the MTI improvement factor as defined in Sec. 15.4. The basis for obtaining the optimum MTI filter is again the covariance matrix of the clutter returns as given by Eq. (15.15). As shown by Capon,[13] the weights of the optimum MTI are found as the eigenvector corresponding to the smallest eigenvalue of the clutter covariance matrix and the MTI improvement factor is equal to the inverse of the smallest eigenvalue.

In Fig. 15.20 the improvement factor of an MTI using the optimum weights is compared with the binomial coefficient MTI for different values of the relative clutter spectral spread and shown as a function of the number of pulses in the CPI. These results again assume a gaussian-shaped clutter spectrum. For typical
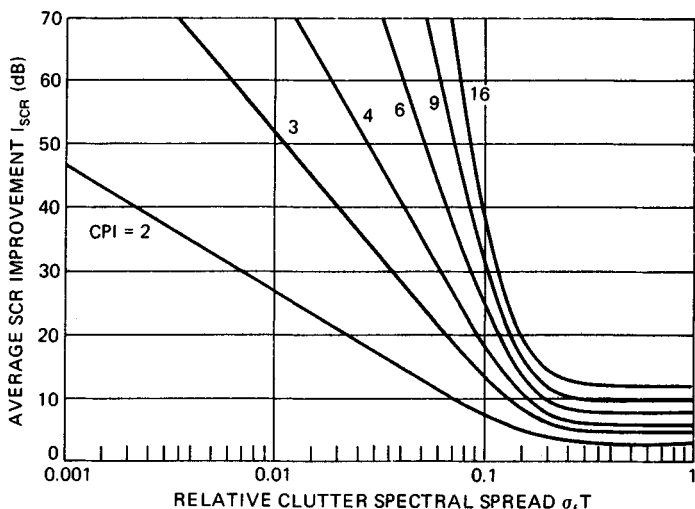
FIG. 15.19 Reference curve of optimum average SCR improvement for a gaussian-shaped clutter spectrum.
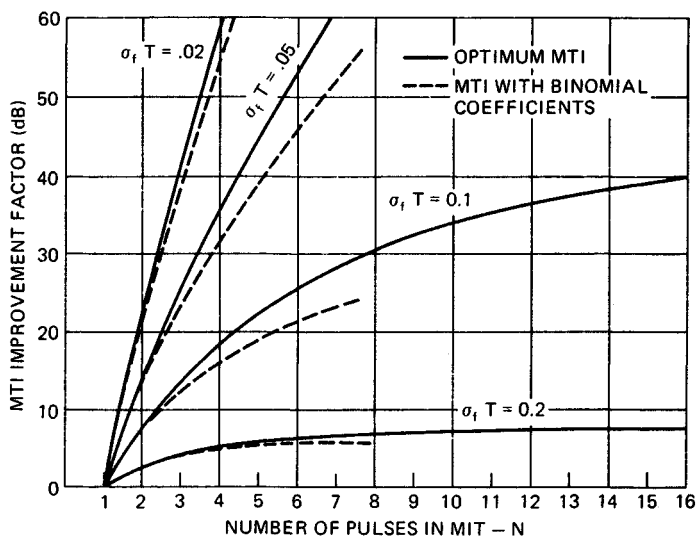

FIG. 15.20 Comparison of MTI improvement factor of binomial-weight MTI and optimum MTI against a gaussian-shaped clutter spectrum.

numbers of pulses in the MTI (three to five) the binomial coefficients are remarkably robust and provide a performance which is within a few decibels of the optimum. Again, it should be noted that any attempt to implement an MTI canceler, which performs close to the optimum, would require the use of adaptive techniques which estimate the clutter characteristics in real time. If the estimate is in

error, the actual performance may fall below that of the binomial-weight MTI canceler.

15.7 MTI CLUTTER FILTER DESIGN

The MTI block diagram shown in Fig. 15.3 and discussed in detail in Sec. 15.2 uses a single-delay canceler. It is possible to utilize more than one delay and to introduce feedback and/or feedforward paths around the delays to change the MTI system response to targets of different velocities. Multiple-delay cancelers have wider clutter rejection notches than single-delay cancelers. The wider rejection notch encompasses more of the clutter spectrum and thus increases the MTI improvement factor attainable with a given clutter spectral distribution.

When a number of single-delay feedforward cancelers are cascaded in series, the overall filter voltage response is $k2^n \sin^n (\pi f_d T)$, where k is the target amplitude, n is the number of delays, f_d is the doppler frequency, and T is the interpulse period.[15] The cascaded single-delay cancelers can be rearranged as a transversal filter, and the weights for each pulse are the binomial coefficients with alternating sign: 1, -1 for two pulses; 1, -2, 1 for three pulses; 1, -3, 3, -1 for four pulses, etc. Changes of the binomial feedforward coefficients and/or the addition of feedback modify the filter characteristics. Within this chapter, reference to *binomial-weight cancelers* refers to cancelers with the $2^n \sin^n (\pi f_d T)$ transfer function.

Figures 15.21 to 15.23 represent typical velocity response curves obtainable from one-, two-, and three-delay cancelers. Shown also are the canceler configurations assumed, with appropriate Z-plane pole-zero diagrams. The Z plane is the comb-filter equivalent of the S plane,[16,17] with the left-hand side of the S plane transformed to the inside of the unit circle centered at $Z = 0$. Zero frequency is at $Z = 1 + j0$. The stability requirement is that the poles of the Z transfer function lie within the unit circle. Zeros may be anywhere.

These velocity response curves are calculated for a scanning radar system with 14.4 hits per beamwidth. An antenna beam shape of $(\sin U)/U$, terminated at the first nulls, was assumed. The shape of these curves, except very near the blind speeds, is essentially independent of the number of hits per beamwidth or the assumed beam shape.

The ordinate, labeled "response," represents the single-pulse signal-to-noise response of the MTI receiver relative to the signal-to-noise response of a normal linear receiver for the same target. Thus all the response curves are normalized with respect to the average gain for the given canceler configuration. The intersection at the ordinate represents the negative decibel value of I, the MTI improvement factor for a point clutter target processed in a linear system.

Because these curves show the signal-to-noise response for each output pulse from the MTI canceler, the inherent loss incurred in MTI processing due to the reduction of the effective number of independent pulses integrated[18] is not apparent. This loss may vary from 1½ to almost 3 dB, depending upon the number of pulses on target. In addition, if quadrature MTI channels (see Sec. 15.12) are not employed, there is an additional loss of 1½ to 3 dB, again depending upon the number of pulses on target.

The abscissa of these curves, V/V_B, represents the ratio of target velocity V to the blind speed $V_B = \lambda f_r/2$, where λ is the radar wavelength and f_r is the average
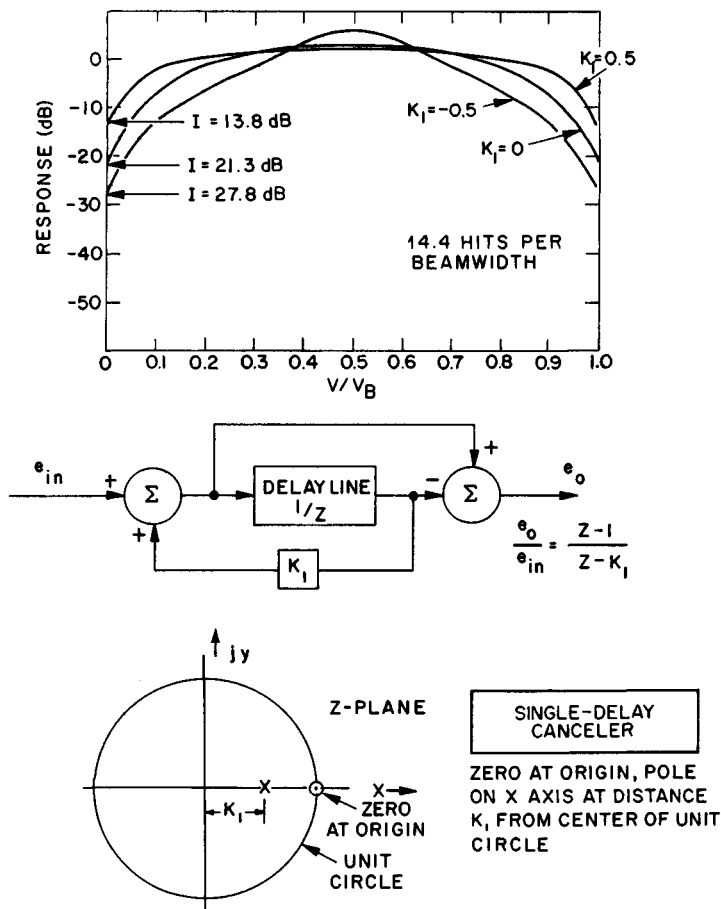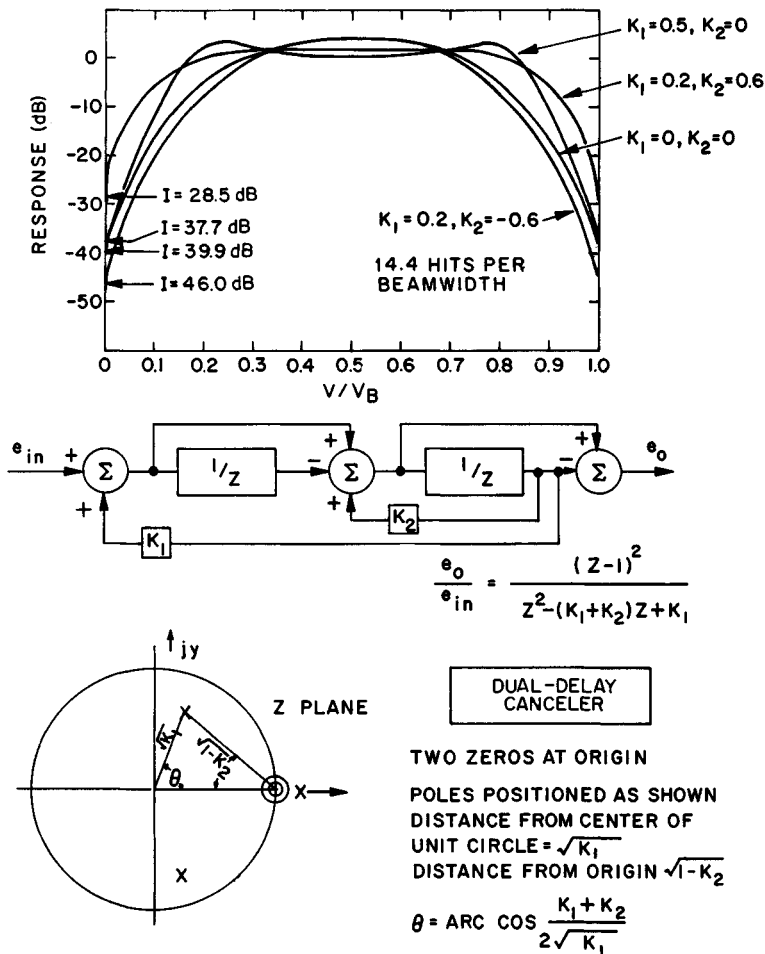
FIG. 15.21 One-delay canceler.

PRF of the radar. The abscissa can also be interpreted as the ratio of the doppler frequency to the average PRF of the radar.

The canceler configurations shown are not the most general feedforward, feedback networks possible but, rather, are practical configurations easy to implement. Many configurations are computationally equivalent. More flexibility in locating zeros and poles is achieved with delays in pairs as shown for the second and third delays of the triple canceler. (In this configuration, the zeros are constrained to the unit circle.)

The triple-canceler configuration is such that two of the zeros can be moved around the boundary of the unit circle in the Z plane. Moving the zeros gives a 4 or 5 dB increase in the MTI improvement factor for specific clutter spectral spreads, as compared with keeping all three zeros at the origin.[19]

It is interesting to note the width of the rejection notches for the different

FIG. 15.22 Two-delay canceler.

binomial-weight canceler configurations. If the −6 dB response relative to normal response is used as the measuring point, the rejection is 24 percent of all target dopplers for the single canceler, 36 percent for the dual canceler, and 45 percent for the triple canceler. Consider the dual canceler, for example. Eliminating 36 percent of the dopplers means limiting the system to a long-term average of 64 percent single-scan probability of detection. Feedback can be used to narrow the rejection notch without much degradation of I. If feedback is used to increase the improvement factor, the single-scan probability of detection becomes worse.

Figure 15.24 shows the effect of feedback on I. These curves are calculated for a $(\sin U)/U$ antenna pattern terminated at the first nulls. The no-feedback curves shown here are almost indistinguishable from the theoretical curves derived for a
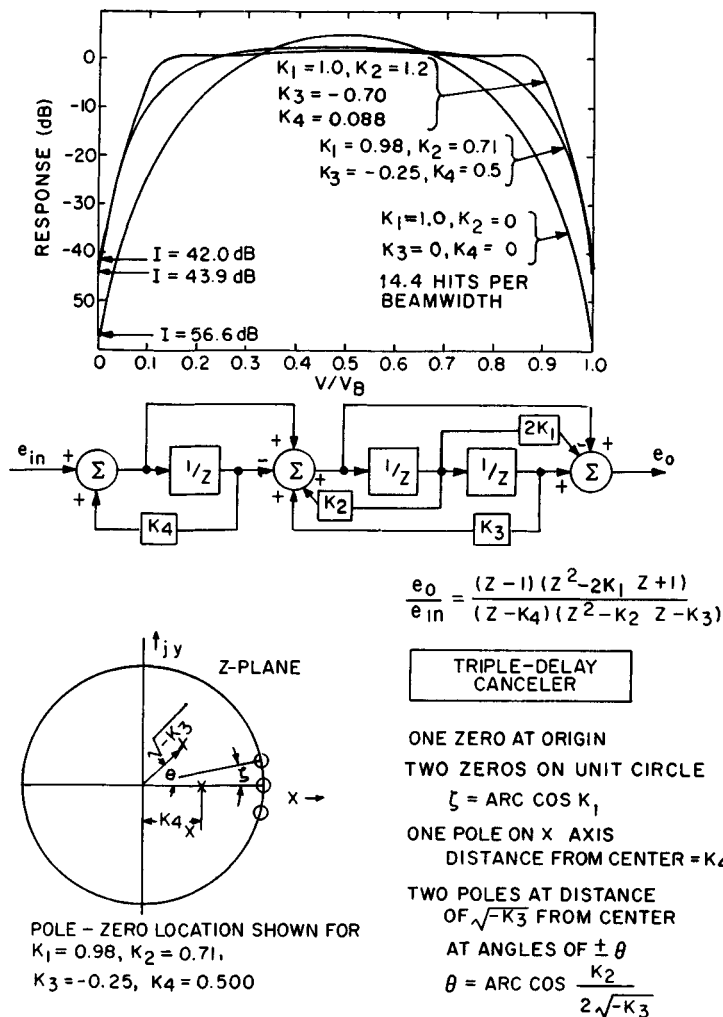
$$\frac{e_0}{e_{in}} = \frac{(Z-1)(Z^2-2K_1\,Z+1)}{(Z-K_4)(Z^2-K_2\,Z-K_3)}$$

TRIPLE-DELAY CANCELER

ONE ZERO AT ORIGIN

TWO ZEROS ON UNIT CIRCLE

    ζ = ARC COS K_1

ONE POLE ON X AXIS
    DISTANCE FROM CENTER = K_4

TWO POLES AT DISTANCE
    OF $\sqrt{-K_3}$ FROM CENTER

AT ANGLES OF $\pm\,\theta$

θ = ARC COS $\dfrac{K_2}{2\sqrt{-K_3}}$

POLE – ZERO LOCATION SHOWN FOR
K_1 = 0.98, K_2 = 0.71,
K_3 = -0.25, K_4 = 0.500

FIG. 15.23 Three-delay canceler.

gaussian pattern shown in Fig. 15.12. (One of the curves showing the effect of feedback on the triple canceler is not straight because two of the three zeros are not at the origin but have been moved along the unit circle the optimum amount for 14 hits per beamwidth. Thus, at 40 hits per beamwidth, these two zeros are too far removed from the origin to be very effective.)

In theory, it is possible to synthesize almost any velocity response curve with digital filters.[16] For each pair of poles and pair of zeros on the Z plane, two delay sections are required. The zeros are controlled by the feedforward paths, and the poles by the feedback paths.

Velocity response shaping can be accomplished by the use of feedforward only,
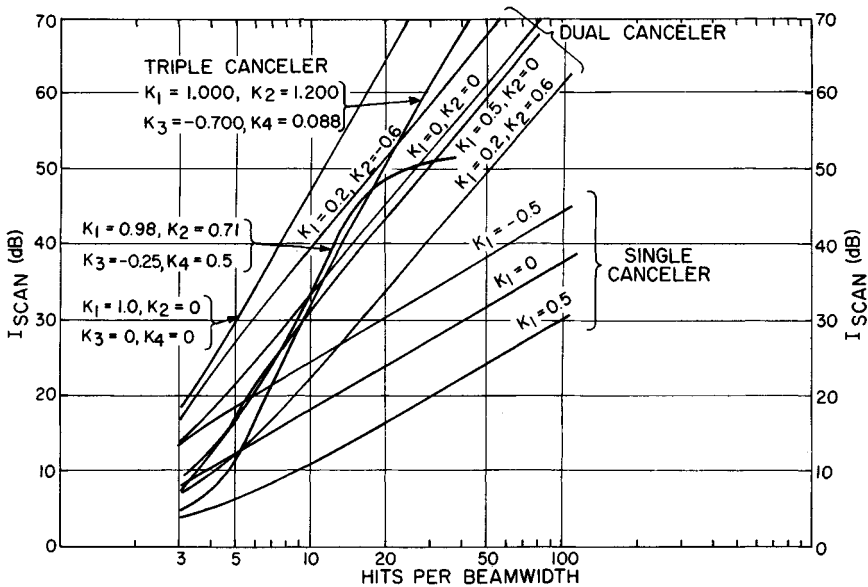
FIG. 15.24 Improvement factor limitation due to scanning for cancelers with feedback, computer-calculated for an assumed antenna pattern of (sin U)/U terminated at the first nulls.

without the use of feedback. The principal advantage of not using feedback is the excellent transient response of the canceler, an important consideration in a phased array or when pulse interference noise is present. If a phased array radar uses a feedback canceler, many pulses may have to be gated out after the beam has been repositioned before canceler transient ringing has settled to a tolerable level. An initialization technique has been proposed[20] to alleviate this problem, but it provides only partial reduction in the transient settling time. If feedforward only is used, only three or four pulses have to be gated out after moving the beam. The disadvantage of using feedforward for velocity response shaping is that an additional delay must be provided for each zero used to shape the response. Also, an inherent loss in improvement factor capability is caused by using zeros to shape the velocity response. This may or may not be significant, depending on the clutter spectral spread and the number of zeros available for cancellation. Figure 15.25 shows the velocity response and Z-plane diagram of a feedforward-only, shaped-response four-pulse canceler. Also shown are the velocity responses of a five-pulse feedforward canceler and a three-pulse feedback canceler. For the cancelers shown, the improvement factor capability of the three-pulse canceler is about 4 dB better than the shaped-response four-pulse feedforward canceler, independent of clutter spectral spread.

The five-pulse canceler response shown is a linear-phase[21] MTI filter described by Zverev.[22] The four zeros are located on the Z-plane real axis at +1., +1., −0.3575, and −2.7972. Much of the literature on filter synthesis describes linear-phase filters, but for MTI applications linear phase is of no importance. Almost identical filter responses can be obtained with nonlinear-phase filters that require fewer pulses, as shown in Fig. 15.25. Because only a fixed number of pulses is available during the time on target, none should be wasted. Thus one should choose the nonlinear-phase filter that uses fewer pulses.
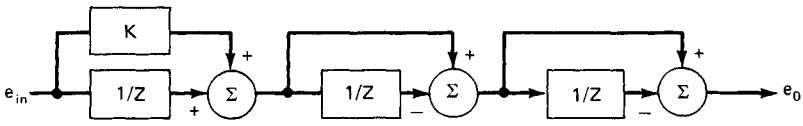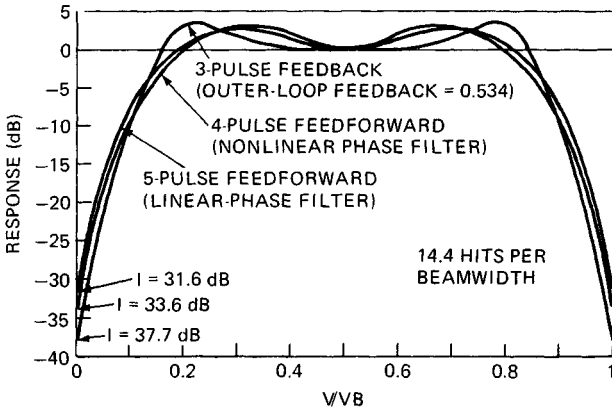
$$\frac{e_0}{e_{in}} = \frac{(Z-1)^2 (Z+\frac{1}{K})}{Z^3}$$
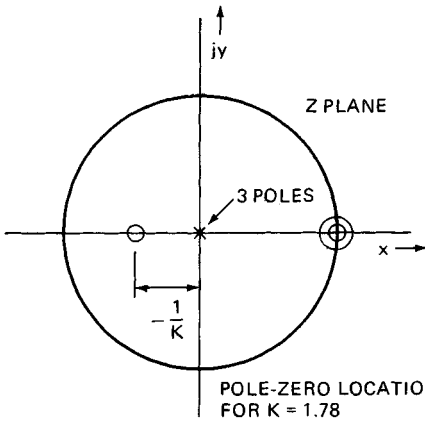
TRIPLE-DELAY
FEEDFORWARD CANCELLER

3 POLES AT CENTER OF UNIT CIRCLE
2 ZEROS AT ORIGIN
1 ZERO ON X-AXIS AT $-\frac{1}{K}$

POLE-ZERO LOCATION SHOWN
FOR K = 1.78

FIG. 15.25 Shaped-velocity-response feedforward cancelers compared with three-pulse feedback canceler. See text for five-pulse canceler parameters.

15.8 CLUTTER FILTER BANK DESIGN

As discussed in Sec. 15.1, the MTD uses a waveform consisting of coherent processing intervals (CPIs) of N pulses at the same PRF and RF frequency. The PRF and possibly the RF are changed from one CPI to the next. With this constraint only finite-impulse-response (FIR) filter designs are realistic candidates for the filter bank design. (Feedback filters require a number of pulses to settle after either the PRF or the RF is changed and thus would not be practical.)

The number of pulses available during the time when a surveillance radar beam illuminates a potential target position is determined by system parameters and requirements such as beamwidth, PRF, volume to be scanned, and the required data update rate. Given the constraint of the number of pulses on target, one must decide how many CPIs should occur during the time on target and how many pulses per CPI. The compromise is usually difficult. One wishes to use more pulses per CPI to enable the use of better filters, but one also wishes to have as many CPIs as possible. Multiple CPIs (at different PRFs and perhaps at different RF frequencies) improve detection and can provide information for true radial velocity determination.[23]

The design of the individual filters in the doppler filter bank is a compromise between the frequency sidelobe requirement and the degradation in the coherent integration gain of the filter. The number of doppler filters required for a given length of the CPI is a compromise between hardware complexity and the straddling loss at the crossover between filters. Finally the requirement of providing a high degree of clutter suppression at zero doppler (land clutter) sometimes introduces special design constraints.

When the number of pulses in a CPI is large (≥ 16), the systematic design procedure and efficient implementation of the fast Fourier transform (FFT) algorithm is particularly attractive. Through the use of appropriate weighting functions of the time-domain returns in a single CPI, the resulting frequency sidelobes can be readily controlled. Further, the number of filters (= the order of the transform) needed to cover the total doppler space (= the radar PRF) can be chosen independently of the CPI, as discussed below.

As the CPI becomes smaller (≤ 10), it will become important to consider special designs of the individual filters to match the specific clutter suppression requirements at different doppler frequencies in order to achieve better overall performance. While some systematic procedures are available for designing FIR filters subject to specific passband and stopband constraints, the straightforward approach for small CPIs is to use an empirical approach in which the zeros of each filter are adjusted until the desired response is obtained. An example of such filter designs is presented below.

Empirical Filter Design. An example of an empirical filter design for a six-pulse CPI follows. (The six pulses per CPI may be driven by system considerations, such as time on target.) Because the filter will use six pulses, only five zeros are available for the filter design: the number of zeros available is the number of pulses minus one. The filter design process consists of placing the zeros to obtain a filter bank response that conforms to the specified constraints. The example that follows was produced with an interactive computer program with which the zeros could be moved until the desired response was obtained. The assumed filter requirements are as follows:

1. Provide a response of −66 dB in the clutter rejection notch (relative to the peak target response) of the moving-target filters.

2. Provide a response of −46 dB for chaff rejection at velocities between ±20 percent of the ambiguous doppler frequency range.

3. Owing to hardware limitations, only five filters will be implemented.

4. Three of the five filters will reject fixed clutter and respond to moving targets. Two filters will respond to targets at zero doppler and its ambiguities. (With good fixed clutter rejection filters, it takes two or more coherent filters to cover the gap in response at zero velocity.)

With the above considerations, a filter bank can be constructed.

Figure 15.26a shows the filter designed to respond to targets in the middle of the doppler passband. The sidelobes near zero velocity are 66 dB down from the peak, thus providing good clutter rejection for clutter within 5 percent of zero doppler. The −46 dB sidelobe provides chaff rejection to ±16 percent. Because of the constraint of only 5 zeros available, this filter could not provide −46 dB rejection to ±20 percent.
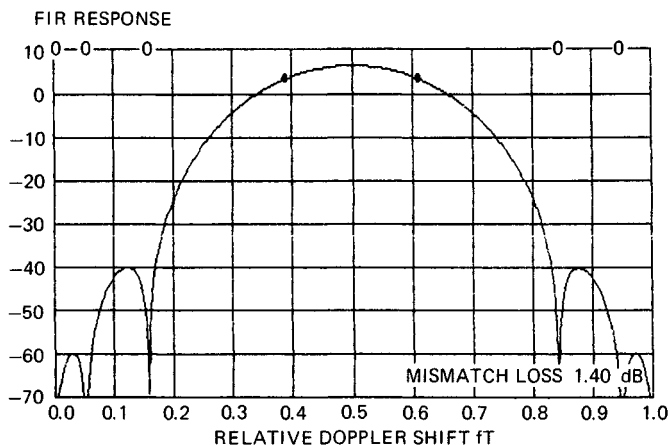

FIG. 15.26a Six-pulse filter for targets at $fT = 0.5$.

Figure 15.26b shows the filter that responds to targets as near as possible to zero doppler, while having zero-doppler response of −66 dB. Two zeros are placed near zero, providing −66 dB response to clutter at zero. The filter sidelobes between 0.8 and 1.0 doppler provide the specified chaff rejection of 48 dB. A mirror image of this filter is used for the third moving doppler filter. (The mirror-image filter has coefficients that are complex conjugates of the original filter coefficients.)

Figure 15.26c shows the first filter designed for response at zero doppler. Considerations here are that the straddling loss of the filter bank be minimized (this dictates the location of the peak), that the response to chaff at 0.8 doppler be down 46 dB, and that the mismatch loss be minimized. Minimizing the mismatch loss is accomplished by permitting the filter sidelobes between 0.3 and 0.8 to rise as high as needed (lower sidelobes in this range increase the mismatch loss). The second zero-doppler filter is the mirror image of this one.
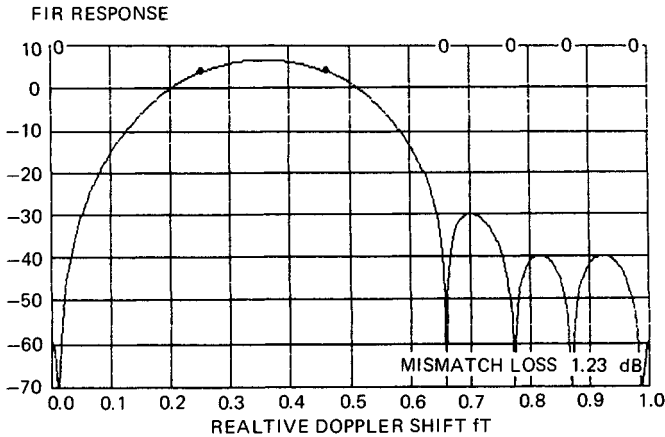
FIR RESPONSE

FIG. 15.26*b*   Six-pulse filter for targets at *fT* = 0.3 that rejects fixed clutter.
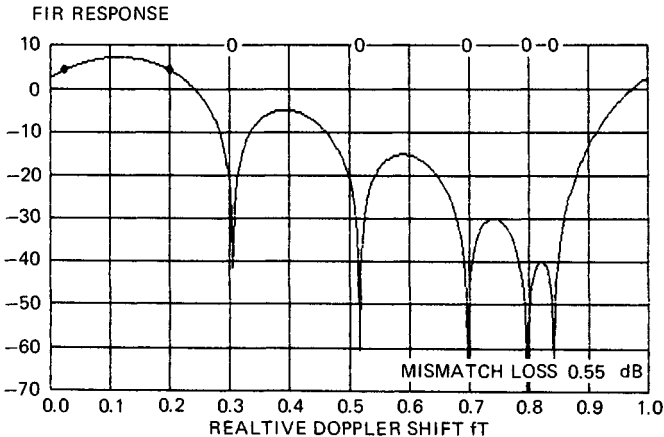
FIR RESPONSE

FIG. 15.26*c*   Six-pulse filter that responds to targets at zero doppler but rejects chaff at *fT* = 0.8.

Figure 15.26*d* shows the composite response of the filter bank. Note that the filter peaks are fairly evenly distributed. The dip between the first zero-doppler filter and the first moving doppler filter is larger than the others, primarily because, under the constraints, it is impossible to move the first doppler filter nearer to zero velocity.

Chebyshev Filter Bank.   For larger number of pulses in the CPI a more systematic approach to filter design is desirable. If a doppler filter design criterion is chosen that requires the filter sidelobes outside the main response to be below a specified level (i.e., providing a constant level of clutter suppression), while simultaneously minimizing the width of the filter response, a filter design based on the Dolph-Chebyshev distribution provides the optimum solution. Properties and design procedures based on the Dolph-Chebyshev distribution can be found in
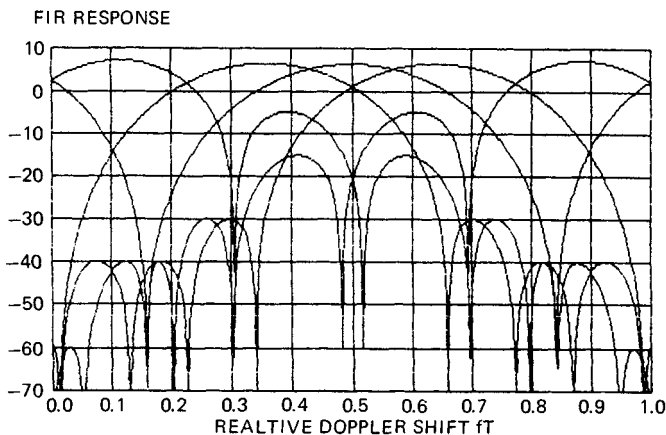
FIR RESPONSE

FIG. 15.26d Composite response of the bank for five six-pulse filters.
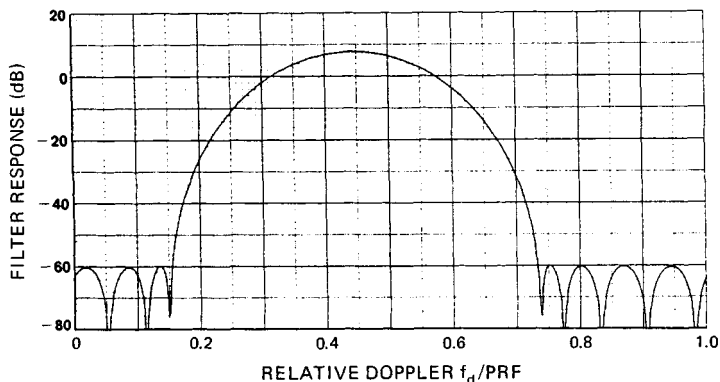

FIG. 15.27 Chebyshev FIR filter design with 68 dB doppler sidelobes.

the antenna literature. An example of a Chebyshev filter design for a CPI of nine pulses and a sidelobe requirement of 68 dB is shown in Fig. 15.27. The peak filter response can be located arbitrarily in frequency by adding a linear-phase term to the filter coefficients.

The total number of filters implemented to cover all doppler frequencies is a design option trading straddling loss at the filter crossover frequencies against implementation complexity. An example of a complete doppler filter bank implemented with nine uniformly spaced filters is shown in Fig. 15.28. The performance of this doppler filter bank against the clutter model considered in Fig. 15.18 is shown in Fig. 15.29. This graph shows the signal-to-clutter ratio improvement against clutter at zero doppler as a function of target doppler frequency. Only the response of the filter providing the largest improvement is plotted at each target doppler. For comparison the optimum curve from Fig. 15.18 is shown by a broken line and thus provides a direct assessment of how well the
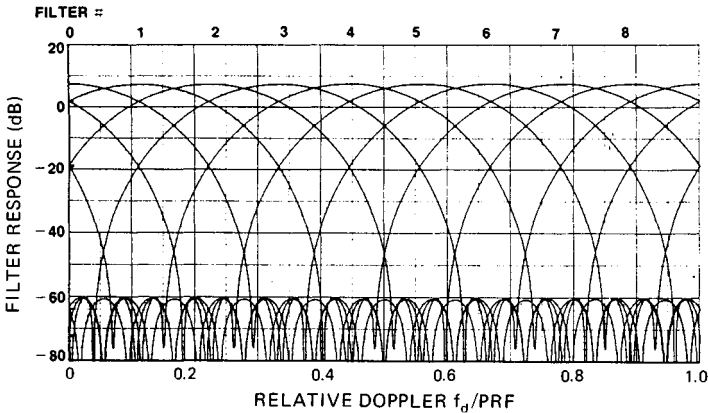
FILTER =

FIG. 15.28   Doppler filter bank of 68 dB Chebyshev filters. CPI = nine pulses.

Chebyshev filter design performs against a given clutter model. Also shown is the average SCR improvement for both the optimum and the Chebyshev filter bank.

Finally, Fig. 15.30 shows the average SCR improvement of the 68 dB Chebyshev doppler filter bank as well as the optimum curve (from Fig. 15.19) as a function of the relative spectrum spread of the clutter. Owing to the finite number of filters implemented in the filter bank, the average SCR improvement will change by a small amount if a doppler shift is introduced into the clutter returns. This effect is illustrated by the cross-hatched region, which shows upper and lower limits on the average SCR improvement for all possible clutter doppler shifts. For a smaller number of filters in the doppler filter bank this variation would be larger.
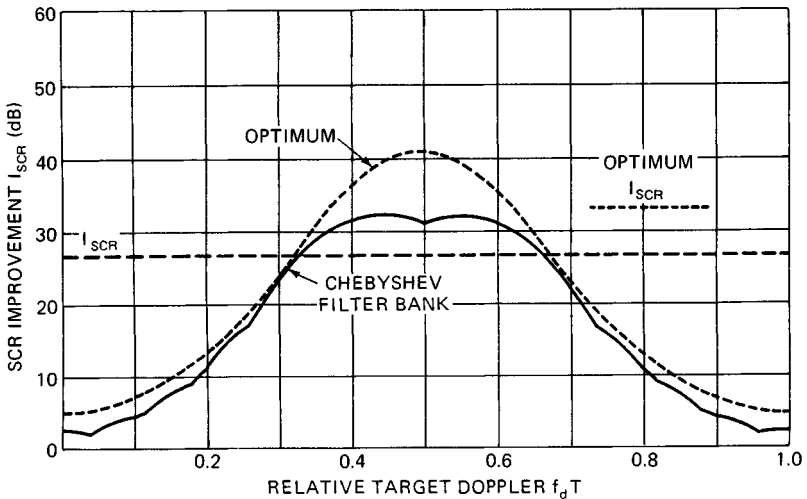

FIG. 15.29   SCR improvement of 68 dB Chebyshev doppler filter bank compared with the optimum.
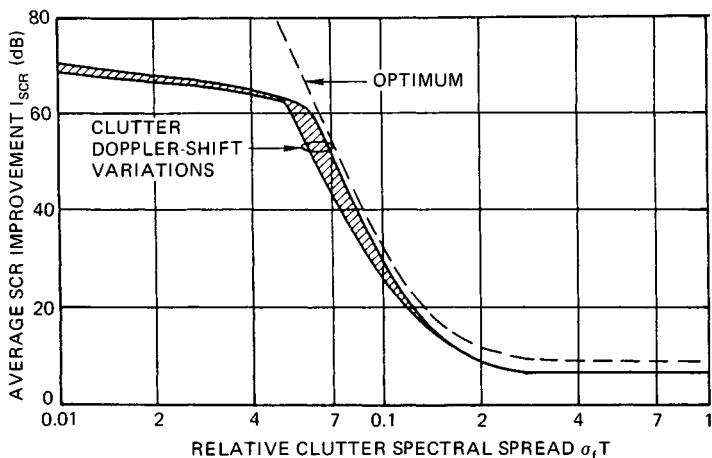
FIG. 15.30 Average SCR improvement for the 68 dB Chebyshev filter bank shown in Fig. 15.28. CPI = nine pulses. Optimum is from Fig. 15.19.

Fast Fourier Transform Filter Bank.   For a large number of parallel doppler filters, hardware implementation can be significantly simplified through the use of the FFT algorithm. The use of this algorithm constrains all filters in the filter bank to have identical responses, and the filters will be uniformly spaced along the doppler axis. The number of filters implemented for a given size of the CPI can, however, be varied. For example, a larger number of filters can be realized by extending the received data with extra zero values (also known as zero padding) after the received returns have been appropriately weighted in accordance with the desired filter response (e.g., Chebyshev).

15.9 STAGGERED PRF

Stagger Design Procedures.   The interval between radar pulses may be changed to shift the target velocities to which the MTI system is blind. The interval may be changed on a pulse-to-pulse, dwell-to-dwell (each dwell being a fraction of the beamwidth), or scan-to-scan basis. Each approach has advantages. The advantages of the scan-to-scan method are that the radar system is easier to build, and multiple-time-around clutter is canceled in a power amplifier MTI system. The transmitter stabilization necessary for good operation of an unstaggered MTI system costs money and weight. To stabilize the transmitter sufficiently for pulse-to-pulse or dwell-to-dwell stagger operation is considerably more difficult. Pulse-to-pulse staggering is used with MTI processing, while dwell-to-dwell staggering is used with filter bank processing.

For many MTI applications pulse-to-pulse staggering is essential. For example, if a binomial-weighted three-pulse canceler which has 36 percent–wide rejection notches is employed and if scan-to-scan pulse staggering is used, 36 percent of the desired targets would be missing on each scan owing to doppler considerations alone. This might be intolerable for some applications. With pulse-to-pulse staggering, good response can be obtained on all dopplers of interest on each scan. In addition, better velocity response can be obtained at some dopplers than